Irradiation effect of yttria-stabilized zirconia by high dose dual ion beam irradiation*

Zhang Yan-Wen(张艳文)[a], Wang Xu(王 绪)[a], Liu Shi-Yi(刘士毅)[a], Tang Mei-Xiong(唐美雄)[a], Zhao Zi-Qiang(赵子强)[a]†, Zhang Peng(张 鹏)[b], Wang Bao-Yi(王宝义)[b], and Cao Xing-Zhong(曹兴忠)[b]

[a] *State Key Laboratory of Nuclear Physics and Technology, Institute of Heavy Ion Physics, Peking University, Beijing* 100871, *China*
[b] *Key Laboratory of Nuclear Analysis Techniques, Institute of High Energy Physics, Chinese Academy of Sciences, Beijing* 100049, *China*

(Received 14 November 2013; revised manuscript received 12 December 2013; published online 20 April 2014)

Yttria-stabilized zirconia (YSZ) is irradiated with 2.0-MeV Au^{2+} ions and 30-keV He^{+} ions. Three types of He, Au, Au + He (successively) ion irradiation are performed. The maximum damage level of a sequential dual ion beam implanted sample is smaller than single Au ion implanted sample. A comparable volume swelling is found in a sequential dual ion beam irradiated sample and it is also found in a single Au ion implanted sample. Both effects can be explained by the partial reorganization of the dislocation network into weakly damaged regions in the dual ion beam implanted YSZ. A vacancy-assisted helium trapping/diffusion mechanism in the dual ion beam irradiated condition is discussed. No phase transformation or amorphization behavior happens in all types of ion irradiated YSZ.

Keywords: irradiation damage, swelling, helium diffusion

PACS: 61.80.–x, 61.80.Jh, 61.82.–d **DOI:** 10.1088/1674-1056/23/6/066105

1. Introduction

Yttria-stabilized zirconia (YSZ) is fabricated by doping the zirconia with yttria. Yttria stabilizes the cubic phase zirconia at room temperature. Due to its high radiation resistance and high chemical stability, YSZ is a suitable model system for investigating the irradiation effects of materials.[1,2] This single crystalline material can be used for the intermatrix layer of nuclear fuel[3] and also for the covering and storage of nuclear waste.[4]

In nuclear reactors, materials are exposed to severe irradiation environment of atomic displacement damage and a large number of helium ions which are generated by neutron irradiation and nuclear transmutation, respectively. Ion beam irradiation is a useful and important technology to simulate the radiation damage or He ion accumulation in nuclear materials. Most of the experimental work on zirconia was performed using heavy ion implantation to simulate the damage induced by neutron radiation[5–9] or by implantation of He ions to simulate the damage caused by α particle.[10–15] Recently the release of He ions from vacancy defects was found in simultaneous dual ion beam (Zr ions and a relatively low fluence of He ions) irradiation.[16] As the actual nuclear material or a part of the equipment, the He content in zirconia will be very high. The He ion behavior is different in the high dose (above 2×10^{16}/cm^2) from in low dose (below 6×10^{15}/cm^2) single He ion irradiation.[11] In this paper, dual ion beam irradiation (Au ions and a high fluence of He ions) is carried out to simulate the irradiation environment in a real nuclear reactor.

2. Experimental details

The ZrO_2 [100] single crystal used in this investigation was doped with 6.5-mol% yttria in order to stabilize the cubic phase. Au ion implantation was carried out with a 2×1.7 MV tandem accelerator at the Institute of Heavy Ion Physics in Peking University. He ion implantation was carried out using an anion implanter at Beijing Normal University. The samples were implanted at room temperature (RT) in a random direction (by tilting the crystals with an angle of 7° relative to the surface normal) with Au^{2+} and He^{+} ions of 2 MeV and 30 keV and ion fluences of 5×10^{15} cm^{-2} and 2×10^{16} cm^{-2}, respectively. The beam current densities of Au and He ions each are 1 μA·cm^{-2} to keep the specimen at room temperature (RT) as far as possible. Au and He ions were irradiated singly or dually on the YSZ specimens. For dual ion beam implantation, Au ion irradiation was performed before He ion irradiation. He ion energy was chosen in order to fit the helium profile to the excess vacancy profile generated by the Au^{2+} ions. The ion-induced damage in the YSZ crystal was determined by Rutherford backscattering spectrometry/channeling (RBS/C) measurements with a collimated 2.022-MeV He^{+} beam. The backscattered particles from the target were accepted by an Au–Si surface barrier detector at a 165° laboratory angle. The energy resolution was around 15 keV. The swelling of the implanted specimen was measured using the step height method by Agilent 5500 atomic force microscopy (AFM) with a Si cantilever operated in the tapping mode. The obtained images were treated with a second-order flattening routine.

*Project supported by the National Basic Research and Development Program of China (Grant Nos. 2010CB832904 and 2010CB832902) and the National Natural Science Foundation of China (Grant No. 91226202).

†Corresponding author. E-mail: zqzhao@pku.edu.cn

© 2014 Chinese Physical Society and IOP Publishing Ltd

Cross-sectional transmission electron microscopy (TEM) micrographs were taken to observe the crystal morphology using a JEM-200CX transmission electron microscope, with an accelerating voltage of 300 kV. Open volume defects in the samples were investigated using the positron annihilation spectroscopy (PAS). Using a continuous positron beam with incident energy (E) ranging from 0.5 keV to 20 keV, we perform Doppler broadening depth profiling in the pristine and irradiated samples. A microscopic Raman spectrometer (L2BRAM ARAMIS) was used to characterize the irradiation effects of the pristine and ion-irradiated specimens at room temperature. The excitation source was a 532-nm laser with power below 5 mW to avoid heating.

3. Results and discussion

Figure 1 shows the implanted ion range and damage distributions calculated by the stopping and range of ions in matter (SRIM) 2013.[17] SRIM calculations indicate that the Au^{2+} implantation and the He^{+} implantation result in maximum damages of 21 displacement per atom (dpa) and 0.7 dpa in ZrO_2, respectively, considering a displacement energy of 40 eV for both Zr and O atoms.[18] Auion implantation can cause excessive vacancy V_{Ex}, which is nearer the surface of YSZ than the excessive interstitial atom R_{Ex}.

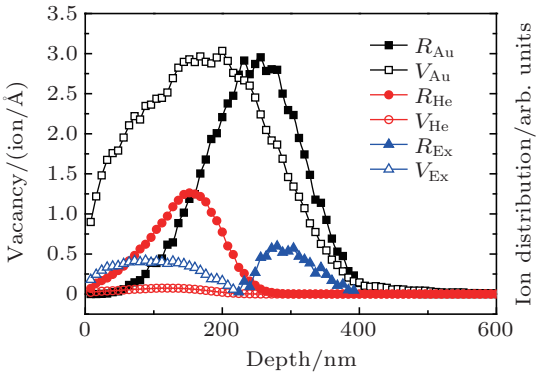


Fig. 1. (color online) Damage and range distributions in YSZ irradiated by 2-MeV Au and 30-keV He ions, calculated by the SRIM 2013 code. The left and right Y axes represent the vacancy and ion distributions caused by per injected Au or He ion at per unit depth (in unit Å), respectively. The distributions of Au and He ions are both in arbitrary units.

Figure 2 shows the RBS/C spectra recorded on pristine, Au, He, and Au + He ion irradiated specimens in order to identify the structural damage and measure the lattice disorder. The random and aligned RBS/C spectrum of the unimplanted specimen included in Fig. 2(a) are for comparison. At the surface peak, the dechanneling yield $\chi_{min} = 6\%$ is measured for the pristine crystal. Such a low value features the high crystalline quality of the original YSZ substrate. The sample implanted with He ions shows an appreciable change near the surface in the channeled spectrum compared with the pristine specimen. That high dose He implantation can cause evident damage was also found by Kuri *et al.*[19] The aligned spectra of Au and Au + He ion implantation both show an enhancement in backscattering yield. The bumps are clearly observed respectively around 1450 keV and 1600 keV in the implanted samples, indicating that the damage is mostly located at a depth corresponding to this energy. The local increase of the dechanneling yield is a consequence of lattice disorder created by ions implantation. Assuming that the observed RBS/C yield is proportional to the number of displaced atoms, we evaluate the damage depth distributions. The measured point defect distribution is shown in Fig. 2(b), which is deduced by a computer program DICADA[20] (dechanneling in crystals and defect analysis) from the channeling data. The damage exhibits two peaks around 120 nm and 220 nm, which correspond to damages created by He and Au ions, respectively.

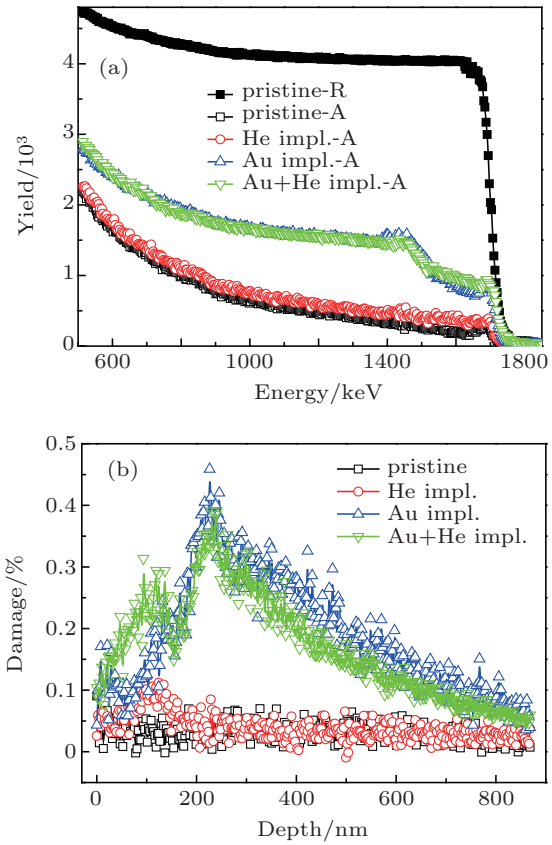


Fig. 2. (color online) (a) Aligned backscattering spectra for the pristine, Au, He, and Au + He ion irradiated specimens. A random spectrum for the unimplanted region is also shown in the figure. (b) The corresponding depth distributions of defects calculated by RBS/C spectrum.

The maximum damage level of the Au + He ion-implanted sample is smaller than that of the Au ion-implanted sample at a depth of 220 nm. A model referred to as multistep damage accumulation (MSDA) was developed to reproduce the damage buildup in many oxide systems.[21] The main assumption of this model relies on the consideration that the damage accumulation results from a series of successive

atomic reorganization steps. Each new step occurs when the current structure of the irradiated material is destabilized by radiation damage. High fluence MeV Au ion implantation also exhibits a surprising decrease in the maximum damage yield, which is attributed to the interaction between previously formed dislocations leading to the disappearance of the tangled dislocation network.[22] The minimum free energy of the system is a whole effect of the sample. The damages in different depths will influence each other. The TEM micrographs of Fig. 3 confirm this statement. Figure 3(a) shows the image of He ion-implanted sample, where point defects and small dislocations can be seen starting to appear. Figure 3(b) shows a dislocation network of tangled dislocations after Au ion implantation. Figure 3(c) reveals the partial reorganization of dislocation network into a weakly damaged region, which mainly consists of fine dislocation loops. This transformation may lead to a decrease in system free energy. Moreover, this microstructural transformation provides an explanation of the surprising decrease in the disorder level observed by RBS/C.

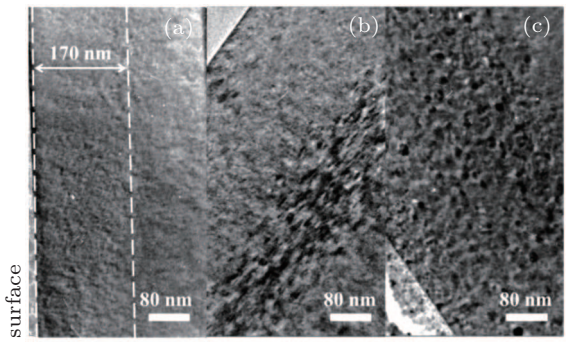


Fig. 3. Bright-field TEM micrographs on YSZ crystals. Panels (a), (b), and (c) are irradiated with He, Au, and Au + He ions respectively.

The swelling of the irradiated YSZ is determined using a step-height method by AFM. The specimen is partially masked by stainless steel with a knife edge during ion irradiation, so that only the unmasked region is irradiated. After irradiation, the surface of the unmasked region becomes elevated and a step forms at the interface between the masked and unmasked regions. AFM three-dimensional (3D) images show the differences in step-height between the areas implanted with He, Au, and Au + He ions and the virgin area in Figs. 4(a), 4(b), and 4(c) respectively. Each of the images is taken over an area of 25 square microns. Many AFM images for one specimen show only small differences among these images. Based on the analysis of several images, the following characteristics are observed. The measurement of this step height provides the total volumetric swelling that has occurred along the path of the injected ions. The swelling in the lateral direction can be ignored because of the anisotropy of the implanted ions. The step heights of He, Au, Au + He ion implanted YSZ are 2.0±0.5 nm, 4.3±0.5 nm, and 4.0±0.5 nm. XRD measurements also show that when Au ion fluence is above $5 \times 10^{15}/\text{cm}^2$, the stress will be released in the 4-MeV Au ion implantation.[22] This effect will reduce the distance of the lattice atoms. Swelling saturation observed under high-dose irradiation accounts for the radiation-induced vacancy emission from extended defects, such as voids, dislocations, and grain boundaries.[23] Macroscopic swelling is mainly related to the densities of dislocations and voids created by interstitial ions and vacancies, respectively.

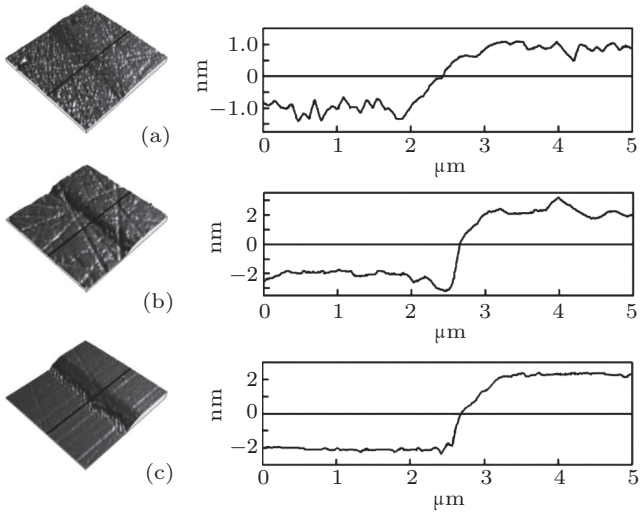


Fig. 4. 3D AFM images of He, Au, Au + He implanted YSZ crystals. A step appears between the irradiated and unirradiated regions. Area coverage is 5 μm×5 μm.

The RBS-C and TEM measurements each show a lower maximum damage level in Au + He ion-implanted sample than that in Au ion-implanted sample. The dislocations created by implanted Au ions absorb more interstitial ions, leading to void growth through absorbing more vacancies, which will result in large swelling. In fact, the difference in swelling between Au and Au + He ion irradiations is very small. The small difference can be attributed to the error of measurement. This means that the swelling degrees are comparable to each other in these two cases.

The Doppler-broadened spectrum is characterized by the *S* parameter that is defined as a ratio of the central region count to the integrated count in the peak (511 keV) and *W* parameter that is defined as a ratio of the peak wing count to the integrated peak count. A high *S* parameter is due to annihilation of the positrons inside the open volume, a high *W* parameter is due to the annihilations of positrons and momentum electrons in the substrate. A positron has a higher possibility to be trapped and annihilated at open volume, because the local electron density is lower due to the reduced atomic density. Figure 5(a) shows the *S* parameter as a function of the positron energy. There is a whole increase in the *S* parameter of the He ion-implanted sample compared with that of the pristine one. The *S* parameter measured in the Au + He ion-implanted YSZ is a little smaller than in the Au ion-implanted

YSZ. The S parameters each as a function of the W parameter are also plotted in Fig. 5(b) in order to compare the open volume defects of this type. All the S–W data points are located on a straight line if there is only one type of open volume defect, which will not be influenced by the concentration difference at different depths.[24,25] There is a sharp kink on the S–W line for He ion implantation, as shown in Fig. 5(b). This can be explained by two types of defects, each of which is comprised of an empty vacancy and a vacancy with He atoms trapped inside.[16] In the Au + He ion-implanted sample, the number of vacancies created by the Au ion is much more than by the He ion. This means that the concentration of He ions in the vacancy is significantly reduced in the Au + He ion-implanted sample. Therefore, the W–S curve of the dual ion beam-implanted sample is closer to the W–S curve of the Au ion-implanted sample, which has no He at all.

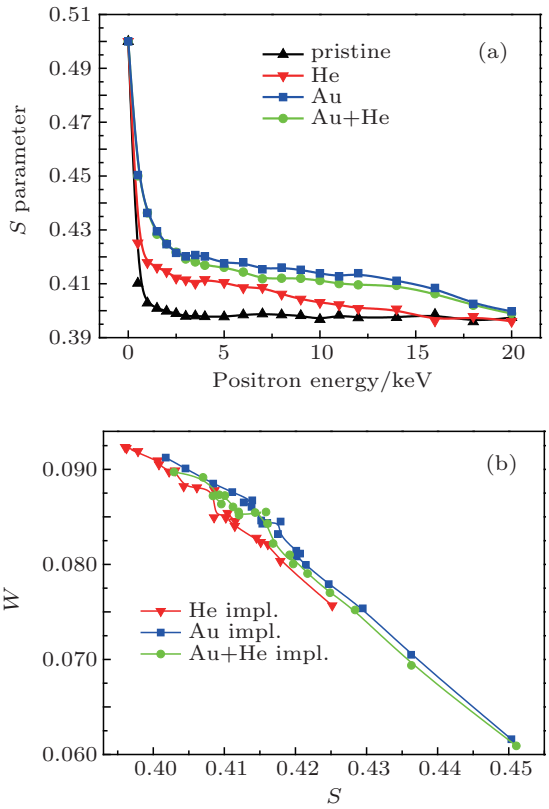


Fig. 5. (color online) (a) Curves of S parameter data versus incident positron energy for pristine, He, Au, Au + He implanted (impl.) YSZ crystals. (b) W–S plot of YSZ crystals irradiated by He, Au, Au + He ion implantation.

In the case of the 2×10^{16}/cm^2 He ion implantation, the damage is created mainly by single vacancy and point defects. The He ions will be trapped mostly in the single vacancy site. The increase in S-parameter after He ion implantation can be caused by single vacancies and vacancy–helium clusters. For 5×10^{15}/cm^2 Au ion implantation, there will be more single vavancies and vacancy clusters. So the S parameter of the Au ion-implanted specimen is very high. In the condition of Au + He ion implantation, the S parameter is similar to that of Au ion implantation. So there is a diffusion phenomenon of He ions. The vacancies can facilitate He ions jumping from one interstitial position to another near-by one via the vacancy, which is around 10% in a $Zr_{0.8}Y_{0.2}O_{1.9}$ crystallattice.[26] Further, He ions are most likely to diffuse by hopping through a single vacancy.[27] The He nucleation and diffusion constitute a competition mechanism. The nucleation and growth of a helium bubble does not seem to happen in the Au + He ion-irradiated sample. The helium bubble does not appear in the TEM image in Fig. 3(c) either. The recombination mechanism has a much lower energy barrier than conventional vacancy diffusion and is efficient for annihilating immobile vacancies in the nearby bulk, resulting in the self-healing of the radiation-induced damage.[28] The void and grain boundaries can act as sinks to self-interstitial atoms formed from nearby displacement cascades.[29] Maybe under the Au + He ion irradiation condition some vacancies and voids will be recombined with interstitial atoms.

Table 1 summarizes the positions of damage peaks created by He and Au ions from different methods. The damage peak of He calculated by SRIM is close to the experimental result. The damage range created by Au ions is about 20 nm as predicted by SRIM, which is a little lower than the value detected by other methods. This is due to the overestimation of the heavy-ion electronic stopping power, which may lead to error in local dose calculation and underestimation of the projected range of slow heavy ions in targets that contain light elements.[30] Generally speaking, the experimental results are coincident with the SRIM calculations.

Table 1. Summary of the damage peak created by Au and He ions using different methods.

Damage peak (He)	Damage peak (Au)
SRIM$\sim$ 120 nm	$\sim$ 200 nm
RBS$\sim$120 nm	$\sim$ 220 nm
PAS $\sim$ 80 nm	$\sim$ 300 nm
TEM $\sim$ 100 nm	$\sim$ 320 nm

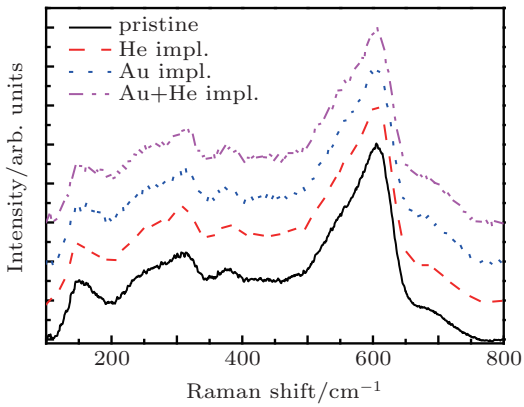


Fig. 6. (color online) Raman spectra of pristine, He, Au, Au + He implanted YSZ crystals.

The Raman spectrum, which is used to distinguish chemical species, can provide valuable evidence for structural properties of materials. It is widely used to investigate the phase transformation and amorphization behavior of ion-irradiated ZrO_2.[31,32] Figure 6 shows the Raman spectra of pristine and ion-irradiated YSZ. No new Raman peak or amorphous region appears in the implanted YSZ compared with in the pristine sample. This illustrates that YSZ is very stable under high dose irradiation damage.

4. Conclusion

In this work, irradiation damage and swelling are detected by RBS, TEM, and AFM. Open volume distribution is detected by PAS. He ions can also create atom displacement damage at high fluence. Dislocation networks of tangled dislocations appear after Au ion implantation. High fluence Au + He ion irradiation can reduce the maximum irradiation damage and swelling. In the Au + He ion implantation, through partial reorganization, the dislocation network can be converted into weakly damaged regions each of which mainly consists of fine dislocation loops. This transformation is controlled by reducing the system free energy. A comparable volume swelling is found between sequential dual ion beam-irradiated samples and single Au ion-implanted samples. In the single He ion-irradiated sample, a helium ion can nucleate with the vacancy. In the Au + He ion-irradiated sample, the He ion nucleation seems not to have happened and some vacancy and void may be recombined with interstitial atoms. The He ion nucleation and diffusion constitute a competition mechanism which is related to the number of vacancies. Damage peak positions created by injected Au and He ions are characterized by different experimental methods. The experimental results are coincident with the SRIM calculations. Neither phase transformation nor amorphization appears in ion-irradiated YSZ. This particularity of YSZ is suitable for making strongly radiation-resistant materials in nuclear reactors with a high fluence-irradiated environment.

Acknowledgment

The authors thank Dr. K Gärtner, Dr. E. Wendler and Sh Y Kong for providing us with the program DICADA.

References

[1] Wu D, Liu C, Zhu X P and Lei M K 2008 *Chin. Phys. Lett.* **25** 1266
[2] Wu D, Liu C, Zhu X P and Lei M K 2009 *Chin. Phys. B* **18** 4976
[3] Thridandapani R R, Folgar C E, Folz D C, Clark D E, Wheeler K and Peralta P 2009 *J. Nucl. Mater.* **384** 153
[4] Couland M, Fourcaudot S, Abril R J, Fernandez-Carretero A and Somers J 2012 *J. Am. Ceram. Soc.* **95** 133
[5] Moll S, Debelle A, Thomé L, Sattonnay G, Jagielski J and Garrido F 2012 *Nucl. Instrum. Method B* **286** 169
[6] Debelle A, Thomé L, Boulle A, Moll S, Garrido F, Qasim L and Rosza P 2012 *Nucl. Instrum. Method B* **277** 14
[7] ThoméL, Moll S, Sattonnay G, Vincent L, Garrido F and Jagielski J 2009 *J. Nucl. Mater.* **389** 297
[8] Jagielski J and ThoméL 2009 *Appl. Phys. A* **97** 147
[9] Yasuda K, Kinoshita C, Matsumura S and Ryazanov A I 2003 *J. Nucl. Mater.* **319** 74
[10] Kuri G, Döbeli M and Gavillet D 2006 *Nucl. Instrum. Method B* **245** 445
[11] Damen P M G, van Veen A, Labohm F, Schut H and van Huis M A 2003 *J. Nucl. Mater. B* **319** 65
[12] Yang T F, Huang X J, Gao Y, Wang C X, Zhang Y W, Xue J M, Yan S and Wang Y G 2012 *J. Nucl. Mater.* **420** 430
[13] Damen P M G, Matzke H J, Ronchi C, Hiernaut J P, Wiss T, Fromknecht R, van Veen A and Labohm F 2002 *Nucl. Instrum. Method B* **191** 571
[14] Costantini J M, Grob J J, Haussy J, Trocellier P and Trouslard P H 2003 *J. Nucl. Mater.* **321** 281
[15] Wiss T A G, Hiernaut J P, Damen P M G, Lutique S, Fromknecht R and Weber W J 2006 *J. Nucl. Mater.* **352** 202
[16] Ou X, Kogler R, Zhou H B, Anwand W, Grenzer J, Hubner R, Voelskow M, Butterling M, Zhou S Q and Skorupa W 2012 *Phys. Rev. B* **86** 224103
[17] Ziegler J F, Biersack J P and Littmark U 1985 *The Stopping and Range of Ions in Solids* (New York: Pergamon)
[18] Sickafus K E, Matzke H J, Hartmann T H, Yasuda K, Valdez J A, Chodak P, Nastasi M and Verrall R A 1999 *J. Nucl. Mater.* **274** 66
[19] Kuri G, Döbeli M and Gavillet D 2006 *Nucl. Instrum. Method B* **245** 445
[20] Gärtner K 2005 *Nucl. Instrum. Method B* **227** 522
[21] Jagielski J and Thomé L 2009 *Appl. Phys. A: Mater. Sci. Process.* **97** 147
[22] Debelle A, Moll S, Décamps B, Declémy A, Thomé L, Sattonnay G, Garrido F, Jozwik I and Jagielskid J 2010 *Scr. Mater.* **63** 665
[23] Dubinko V I, Hu S, Li Y, Henager C H and Kurtz R J 2012 *Phlos. Mag.* **92** 4113
[24] Triftshäuser W 1975 *Phys. Rev. B* **12** 4634
[25] Liskay L, Corbel C, Baroux L, Hautojarvi P, Brinkman A W and Tatarenko S 1994 *Appl. Phys. Lett.* **64** 1380
[26] Ben-Michael R, Tannhauser D S and Genossar J 1991 *Phys. Rev. B* **43** 7395
[27] Zhang P, Lu Y, He C H and Zhang P 2011 *J. Nucl. Mater.* **418** 143
[28] Bai X M, Voter A F, Hoagland R G, Nastasi M and Uberuaga B P 2010 *Science* **327** 1631
[29] Samaras M, Hoffelner W and Victoria M 2006 *J. Nucl. Mater.* **352** 50
[30] Chang Y Q, Zhang Y W, Zhu Z H, Edmondson P D and Weber W J 2012 *Nucl. Instrum. Method B* **286** 173
[31] Gazzoli D, Mattei G and Valigi M 2007 *J. Raman Spectrosc.* **38** 824
[32] Huy L D, Laffez P, Daniel P, Jouanneaux A, Khoi N T and Siméone D 2003 *Mater. Sci. Eng. B* **104** 163